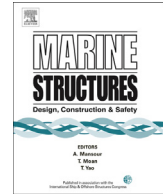




Contents lists available at ScienceDirect

## Marine Structures

journal homepage: [www.elsevier.com/locate/marstruc](http://www.elsevier.com/locate/marstruc)



# A simple parametric formulation for the seabed trench profile beneath a steel catenary riser



Kunpeng Wang<sup>a, b</sup>, Ying Min Low<sup>a, \*</sup>

<sup>a</sup> National University of Singapore, Department of Civil and Environmental Engineering,  
1 Engineering Drive 2, Singapore 117576, Singapore

<sup>b</sup> School of Naval Architecture and Ocean Engineering, Jiangsu University of Science and Technology,  
Zhenjiang 212003, Jiangsu, China

### ARTICLE INFO

#### Article history:

Received 31 July 2015

Received in revised form 15 October 2015

Accepted 22 October 2015

Available online xxx

#### Keywords:

Steel catenary riser

Seabed

Trench

Fatigue analysis

Constrained optimization

### ABSTRACT

Seabed trench has a profound influence on the fatigue performance of a steel catenary riser (SCR) at the touchdown zone. At present, the most well-regarded approach for simulating the complex trench development process is by applying a nonlinear hysteresis seabed contact model, which is time consuming. Field observations have indicated that the trench depth almost stabilizes after a few months following installation. Hence, for practical fatigue design, it is expedient to specify an initial static trench profile to perform the dynamic simulations. This paper presents a new simple parametric formulation for delineating an initial trench profile, as there appears to be no such approach in the literature. The formulation entails two unknown trench parameters (trench length and global trench position), which can be determined using a new iterative static analysis method proposed herein. However, the analysis involves solving a constrained optimization problem, and is not ideal for practical applications. Thus, a surrogate model is devised, by approximating the trench parameters as multivariate polynomial functions of three dimensionless variables of the SCR. A case study comparing the trenches obtained from seabed contact model, static analysis, and surrogate model, shows that the different trench profiles and the associated maximum fatigue damage are in close agreement.

© 2015 Elsevier Ltd. All rights reserved.

\* Corresponding author. Tel.: +65 6516 4127; fax: +65 6779 1635.  
E-mail address: [ceelowym@nus.edu.sg](mailto:ceelowym@nus.edu.sg) (Y.M. Low).

## 1. Introduction

Steel catenary riser (SCR) is a technically feasible and cost-effective option for transportation of hydrocarbons, and it is widely used in many deepwater fields. In the SCR design, fatigue assessment at the touchdown zone (TDZ) is one of the most challenging issues. At the TDZ, the fatigue damage is most pronounced, and also most difficult to predict accurately due to many complex mechanisms involved, such as slug flow, vortex-induced vibration, and SCR-seabed interaction. The effect of seabed interaction can be broadly classified into three aspects, namely soil stiffness, soil suction, and seabed trench, all of which have significant influence on the fatigue performance at the TDZ [1,2]. This paper focusses on the seabed trench, which develops progressively beneath the SCR owing to repeated contact.

One of the earliest research efforts on SCR-seabed interaction are the STRIDE and CARISIMA joint industry projects (JIPs) [1,3], in which full scale field tests were conducted. Some observations were reported, including trench development and nonlinear hysteretic relationship between seabed resistance and riser penetration. The JIPs spurred subsequent research on SCR-soil interaction, and there is still intensive interest on this topic today. Recent experimental studies include Elliott et al. [4], who performed centrifuge tests, and Wang et al. [5], who carried out large scale indoor tests. Trench development is a highly complex process involving interactions between the fluid, structure and soil. Numerical techniques have been developed to simulate this process. Sen and Haser [6] carried out SCR global analysis, in which the local SCR-seabed interaction was simulated by Abaqus/Explicit. Clukey et al. [7] investigated the seabed response and trenching due to riser loading using ANSYS/LS-DYNA, and the results were compared with laboratory tests.

Undoubtedly, experimental tests and detailed numerical analysis are time consuming and costly. Therefore, researchers have developed semi-empirical SCR-soil models, which can be easily incorporated into global dynamic analyses. Aubeny and Biscontin [8,9] proposed empirical formulas for the seabed plastic deformation, and a  $P$ - $y$  model that accounts for the initial penetration, uplift and re-penetration. Several researchers [2,10] have applied the models by Aubeny and Biscontin for fatigue analysis of SCR at the TDZ. Randolph and Quiggin [11] proposed a nonlinear hysteretic seabed model, which has been validated with experimental data [12], and can be used to simulate trench development. To better reflect the seabed degradation, this model gave relatively smaller seabed resistance than the initial  $P$ - $y$  curve at the trench bottom for the re-penetration curve. Randolph and Quiggin's seabed model has been incorporated into the commercial software Orcaflex, which is widely used for riser dynamic analysis. Subsequently, many researchers [13–16] have applied this seabed model for SCR fatigue analysis, either within Orcaflex, or in conjunction with other riser dynamics codes.

The collective efforts of the abovementioned research studies have firmly established the importance of seabed trench on SCR fatigue behavior at the TDZ. The empirical seabed models can be used to simulate the development of trench profile caused by repeated SCR-seabed contact; however, the simulations are computationally demanding due to the slow rate of trench development. Field observation by remote operated vehicle (ROV) in Gulf of Mexico indicated that the trench depth tends to stabilize after reaching four to five times the riser diameter after a few months following the SCR installation [17]. Since a few months constitutes only a small fraction of the total design life of a riser (typically 20 years), in practical fatigue design, it is expedient to specify an initial static trench profile to perform the dynamic simulations. However, so far there appears to be no simple and reasonable approach to determine the initial trench. One reason is that ROV recordings are limited and the trench creation speed depends on the nature of the environmental loads, among other factors.

Clearly, the specified trench profile needs to be realistic. Shiri [18] asserted that unrealistic formulation of the trench may be the reason that some previous studies reported conflicting results for the trench effect on fatigue damage. Several authors have proposed parametric formulas for the trench profile, for example cubic polynomial model [8], quadratic exponential model [18], shifted lognormal distribution [19]. However these formulas have not been validated, and the selection of the parameters of the formulas is also an unresolved issue. Motivated by practical needs, this paper aims to develop a parametric formulation for the trench profile that is straightforward to apply. The trench profile can

then be specified at the start of an SCR dynamic analysis. The formulation will be compared with the penetration profile obtained by the nonlinear hysteretic seabed model by Randolph and Quiggin [11].

## 2. Review of literature

### 2.1. Nonlinear hysteretic seabed contact model

The hysteretic seabed contact model developed by Randolph and Quiggin [11] was validated with test data, and is presently the most well-regarded nonlinear seabed interaction model available. Moreover, it is integrated into the commercial package Orcaflex. Hence, the proposed trench profile will be benchmarked against this hysteretic seabed model, whose features are briefly summarized below.

The model has four contact modes, specifically not-in-contact, initial penetration, uplift and re-penetration. Fig. 1 plots the seabed reaction force against the penetration depth  $z$ . When the riser first comes into contact with the soil, the curve follows the initial penetration curve, up to an arbitrary point labeled “X”. During uplift, the soil resistance rapidly decreases, and becomes negative, indicating suction. When the riser descends again, the re-penetration mode is activated, and the curve may follow the path of (a) or (b). The ultimate resistance is reached at a depth that exceeds the previous penetration depth, reflecting an incremental deepening of the trench. Over time, the trench development manifests through successive series of uplift and re-penetration. Table 1 presents the model parameters and values used in this study.

### 2.2. Existing trench models

The seabed trench beneath the riser would develop gradually under the effect of SCR-seabed interaction. According to field observations, the maximum depth of the trench typically reaches  $4D$  to  $5D$  (where  $D$  is the SCR outer diameter) after several months following the installation [17], although in extreme cases,  $10D$  has been observed. In addition, Bridge and Howells [20] reported that the trench can be described as ladle-shaped in profile, and bell-mouth in plan.

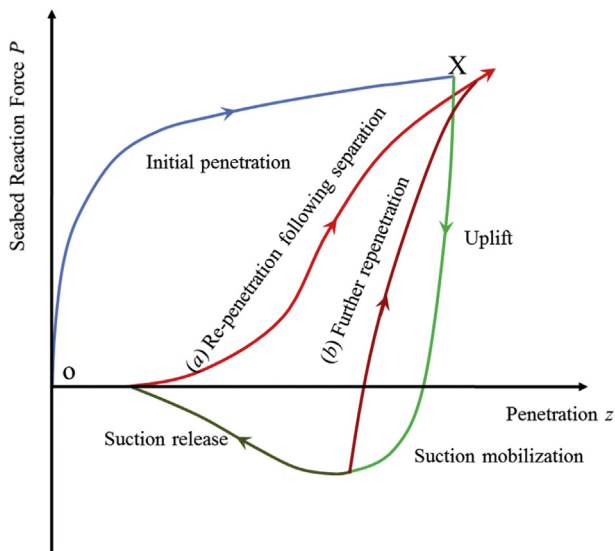


Fig. 1. Sketch of nonlinear pipe–soil interaction model.

**Table 1**  
Parameters of nonlinear pipe–soil interaction model.

Parameter	Value
Mudline shear strength, $S_{u0}$ (kPa)	1.5
Shear strength gradient, $\rho$ (kPa/m)	2.5
Power law parameter, $a$	6.5
Power law parameter, $b$	0.25
Normalized maximum stiffness, $K_{max}$	200
Suction ratio, $f_{suc}$	0.6
Suction decay parameter, $\lambda_{suc}$	0.5
Repenetration parameter, $\lambda_{rep}$	0.4

Fig. 2 sketches a typical trench profile and the SCR resting on the seabed. The profile starts at the trench beginning point (TBP) and terminates at the trench end point (TEP). The touchdown point (TDP) is defined as the location where the SCR first comes into contact with the soil. The trench maximum depth point (TMP) is self-explanatory. Several researchers have proposed parametric equations for describing the trench profile. Let  $\hat{x}$  represent the distance to TBP, and  $d(\hat{x})$  is the trench depth at  $\hat{x}$ . Aubeny and Biscontin [8] proposed a cubic polynomial model given by

$$d(\hat{x}) = d_{max} [c_1(\hat{x}/L_T)^3 + c_2(\hat{x}/L_T)^2 + c_3(\hat{x}/L_T)]$$

$$c_1 = -(2\lambda - 1)/[\lambda(\lambda - 1)]^2, \quad c_2 = (3\lambda^2 - 1)/[\lambda(\lambda - 1)]^2$$

$$c_3 = -(3\lambda^2 - 2\lambda)/[\lambda(\lambda - 1)]^2, \quad \lambda = L_{max}/L_T \tag{1}$$

where  $d_{max}$  is the maximum penetration depth,  $L_{max}$  the horizontal length from TBP to TMP, and  $L_T$  the trench length. Shiri [18] proposed a quadratic exponential model

$$d = d_{max} \left[ \frac{\hat{x}}{L_{max}} e^{(1-\hat{x}/L_{max})} \right]^2 \tag{2}$$

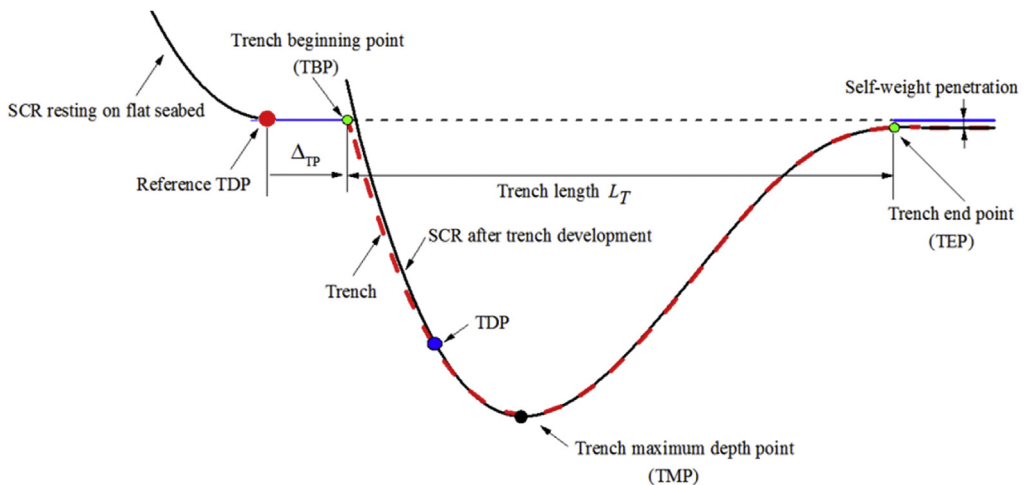


Fig. 2. Sketch of typical seabed trench profile.

It is clarified that trench profiles described by the parametric trench models is prior to the addition of self-weight, whereas the profiles depicted in Fig. 2 includes the self-weight penetration that is formed during static analysis. It is presumed that the SCR self-weight has negligible effect on the maximum trench depth when statically resting on the initial trench, as will be demonstrated in the following section.

For Eq. (1), it is necessary to determine  $L_{\max}$  and  $L_T$  for a prescribed  $d_{\max}$ . By specifying the trench slope at TEP to be zero, the relationship between  $L_{\max}$  and  $L_T$  can be established as

$$L_{\max} = \frac{L_T}{3} \quad (3)$$

This relationship is to some extent in good agreement with the trenches reported by Bridge et al. [3]. For Eq. (2), Shiri [18] defined the trench surface point as the point at which  $d$  falls within 1% of  $d_{\max}$ , and subsequently obtained  $L_{\max} = L_T/5$ .

The maximum penetration depth  $d_{\max}$  is specified by the analyst, for example,  $4D$  to  $5D$  as mentioned earlier. Consequently,  $L_T$  becomes the only unknown variable for the cubic polynomial and quadratic exponential models. However, even if the geometry of the trench is fully defined, the trench position relative to SCR still needs to be determined, and this entails another unknown variable. It is convenient to define the TBP with reference to a known prominent location, which is selected as the TDP for the case of a flat rigid seabed with no trench (see Fig. 2). For the purpose of future reference, this study defines  $\Delta_{TP}$  as the distance between the TBP and the TDP for flat seabed, as illustrated in Fig. 2. The convention is established such as a negative  $\Delta_{TP}$  signifies that the TBP is on the left-hand side of the TDP for flat seabed. This convention implies that with increasing  $\Delta_{TP}$ , the TBP moves towards the right.

Li and Low [19] proposed to model the trench profile following the shape of a shifted lognormal distribution, i.e.

$$d(\hat{x}) = \frac{\beta}{(\hat{x} - \gamma)\sqrt{2\pi\sigma}} \exp\left\{-\frac{1}{2\sigma^2}[\ln(\hat{x} - \gamma) - \mu]^2\right\}, \quad \hat{x} \geq \gamma \quad (4)$$

where  $\mu$  and  $\sigma$  are the parameters of the conventional lognormal distribution,  $\gamma$  is an additional location parameter, and the scale factor  $\beta$  is introduced so that the prescribed  $d_{\max}$  is satisfied. The drawback of the shifted lognormal model, at least for the present purpose, is that it depends on too many parameters, and moreover there is no relationship to  $L_T$ , which is a key trench property. Hence, the shifted lognormal model will not be further investigated in this study.

### 3. Preliminary simulations

The objective of this section is to perform preliminary simulations to better understand the trench development process, ascertain which parametric form is most suitable for describing the trench profile, and to investigate how the trench parameters influence the fatigue behavior.

#### 3.1. Comparison of parametric trench models

Consider an SCR attached to a floating platform, as illustrated in Fig. 3. The global coordinate system is defined such that the origin is located on the seabed directly below the hang-off position. Table 2 lists the main parameters of the SCR. To better understand the trench development process, time domain analysis is performed using Orcaflex (version 9.7), in conjunction with the nonlinear hysteretic seabed model. Orcaflex has the option to include the impact of soil damping, which is not considered in the seabed contact model by Randolph and Quiggin [11]. In this work, soil damping is set to zero in the software. The platform is given a harmonic heave and surge motion, both of 1 m amplitude and 10 s period. Subsequently, the amplitudes are increased to 1.5 m, and another simulation is performed to study the effect of platform motion amplitude on the seabed trench.

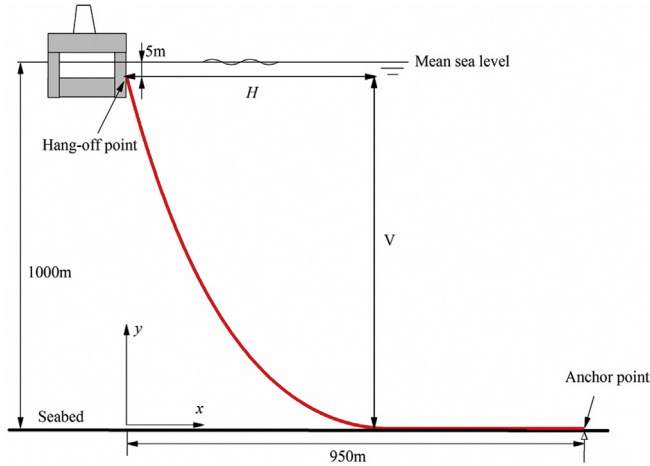


Fig. 3. Typical SCR system.

Fig. 4(a) compares the trench profiles associated with different motion amplitudes, when the maximum depth has reached about  $0.6D$ . The time taken to reach this maximum depth are 1.5 h and 150 s for the cases with 1 m and 1.5 m amplitudes respectively. As expected, with a larger motion amplitude, the trench develops faster. It is also observed from Fig. 4(a) that larger amplitude leads to a slightly increased trench length. However, the trench length increment is trivial compared to the proportional increase in motion amplitude, from which it can be inferred that the motion amplitude primarily affects the trench development speed. Soil damping may in principle also alter the trench development speed; however an investigation of this effect is outside the scope of the present work.

Fig. 4(b) depicts the trench profile at different times for the case with 1 m motion amplitude. The trench requires 1.5 h to reach  $d_{\max} = 0.6D$  from the initial state, but an additional 7.5 h elapses before  $d_{\max}$  becomes  $0.71D$ . This implies that trench development is a slow process, and more importantly, it becomes progressively slower, which explains why the trench tends to stabilize after a certain depth. In addition, Fig. 4(b) shows that the TDP is not located at the seabed surface, but beneath it. The encircled part illustrates that the SCR visibly penetrates the soil from the TDP to TMP, indicating that the stationary seabed reaction forces in this region is substantial.

When the trench depth is  $0.71D$ , the trench length obtained from the simulation is 46 m. The profiles for the parametric models (cubic polynomial and quadratic exponential) can be defined by assigning  $L_T = 46$  m, and aligning the TBP (and consequently also the TEP). Fig. 5 compares the trench profiles obtained by different approaches. The parametric trench profiles are inclusive of self-weight. It is evident that the cubic polynomial model gives much better agreement with the simulated penetration profile compared to the quadratic exponential model. The maximum trench depths for the parametric models appear to be slightly more than the simulated trench. The reason is that the original

**Table 2**  
Key parameters of the SCR.

Parameter	Value
Water depth (m)	1000
Total riser length (m)	1610
Outer diameter (m)	0.3
Inner diameter (m)	0.268
Mass per unit length (kg/m)	175
Elastic modulus (GPa)	210
Morison drag coefficient, $C_D$	0.7
Morison added mass coefficient, $C_A$	1.0

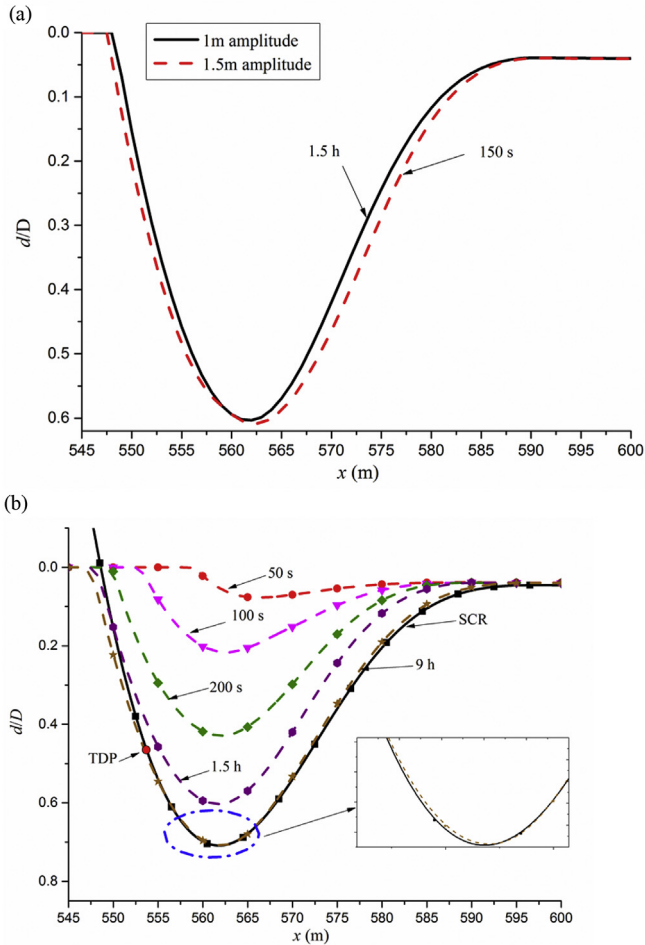


Fig. 4. Trench profiles obtained by simulation: (a) comparison of different motion amplitudes; (b) different simulation durations.

equations do not include self-weight. In other words, the depth of  $0.71D$  is specified prior to the effect of self-weight, thus the final trench profile is slightly greater than  $0.71D$  when self-weight is included. However, this disparity is small in comparison with the trench depth, and may be taken as negligible.

### 3.2. Influence of trench profile on fatigue damage

Fig. 4(b) confirms that trench development is a very slow process. Considering the constraints of computational time in practical design, and the significant influence of seabed trench on the fatigue behavior, it is imperative to set up a plausible initial trench for accurate fatigue prediction. In what follows, a series of simulations are performed to better understand the sensitivity of the fatigue damage to the trench profile. Here, the sea state is characterized by the JONSWAP spectrum [21], with significant waveheight  $H_S = 4.5$  m and spectral peak period  $T_p = 7.5$  s. The irregular waves are unidirectional and propagate in the plane of the riser; consequently only the surge, heave, and pitch motions are excited. For simplicity, only the first-order wave-frequency loads and responses are considered; the second-order slow drift motions are neglected (the implications will be discussed later in Section 4.3).

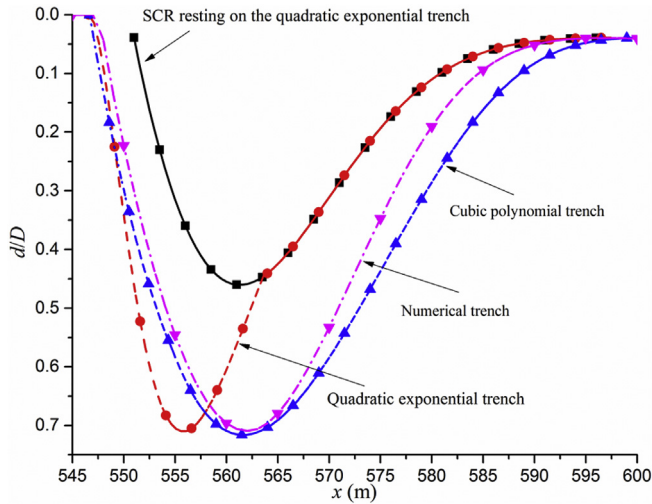


Fig. 5. Comparison of trench profiles obtained by different models.

A global dynamic analysis can be either coupled or uncoupled. In a coupled analysis, the floater, moorings and risers are analyzed simultaneously in one model. Coupled analysis, which simulates the floater, moorings and risers simultaneously in one model, is rigorous but too time consuming for the present application. Hence, for simplicity, an uncoupled analysis is performed, meaning that the platform motions are defined by response amplitude operators (RAOs). The dynamic influence from the moorings and risers are not explicitly modeled, but is assumed to be already incorporated into the RAOs.

The fatigue assessment follows the classical *S–N* curve approach. The DNV Class D *S–N* curve [22], with intercept  $\log(\bar{\sigma})$  and inverse slope  $m = 3$  is selected. Since the time histories of the stresses are irregular, rainflow counting [23] is used to extract the stress ranges, and the total damage is summed using Miner's rule [24]. Dynamic analyses are performed using different trench models shown in Fig. 5. Fig. 6 plots the fatigue damage along the SCR near the touchdown region, for different trench models.

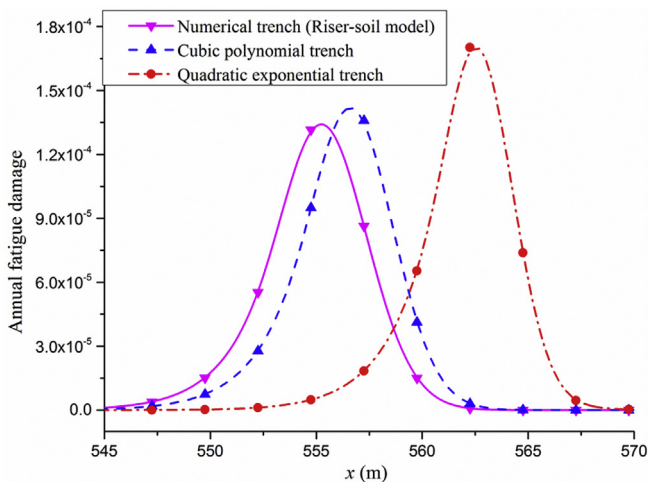


Fig. 6. Annual fatigue damage near TDP under different trench models.

The quadratic exponential trench is found to overestimate the maximum damage compared to the numerical trench, while the location of the maximum damage is also different. In contrast, the fatigue damage associated with the cubic polynomial trench is in much better agreement. Hence, the methods proposed in the work will be based on the cubic polynomial trench, which has two parameters  $L_T$  and  $\Delta_{TP}$ .

It is of interest to study the sensitivity of the fatigue damage to  $L_T$  and  $\Delta_{TP}$ . Suppose that  $d_{\max} = 4D$ . Using an iterative static analysis method that will be detailed in Section 4.1, the trench parameters are found to be  $L_T = 87$  m and  $\Delta_{TP} = -31.6$  m, and the corresponding trench profile is plotted in Fig. 7. It is seen that the TDP is not located at the seabed surface, just as the numerical result in Fig. 4(b). Moreover, it is noted that the shape of the SCR follows closely that of the trench. The trench in Fig. 7 is taken as a baseline case to vary  $L_T$  and  $\Delta_{TP}$ .

Fig. 8(a) illustrates the trench and SCR shapes in which  $L_T$  is varied, keeping TMP constant. If  $L_T$  decreases to 60 m, the SCR will be supported by the two trench ends, and a gap between the SCR and soil manifests between the TDP and TEP. However, if  $L_T$  is increased to 100 m, the fore part of the trench will be separated from the SCR, which is also unrealistic. Moreover,  $L_T$  also influences the fatigue damage, as shown in Fig. 8(b). Overestimation or underestimation of  $L_T$  may lead to a conservative fatigue assessment. For the case of  $L_T = 60$  m, due to the intensive contact at the fore part of the trench, the damage is over predicted in this region. Likewise, for  $L_T = 100$  m, because of the reduced contact area, the dynamic stresses are magnified.

The variation of  $\Delta_{TP}$  has significant impact on the SCR shape at the TDZ, as exemplified in Fig. 9(a). Recalling that  $\Delta_{TP} = -31.6$  m is the optimal value, when the entire trench profile is shifted about 20 m towards the hang-off point ( $\Delta_{TP} = -51.6$  m), the SCR only rests on the rear portion of the trench, as shown in Fig. 9(a), left diagram. This reduces the contact area and amplifies the maximum fatigue damage, which is plotted in Fig. 9(b). When the trench profile is translated about 20 m away from the hang-off point ( $\Delta_{TP} = -11.6$  m), the SCR is subjected to severe reaction forces at the fore portion, which would be compressed, as shown in Fig. 9(a), right diagram. Subsequently, the middle part of the SCR loses seabed support, and the maximum fatigue damage is augmented.

The foregoing results demonstrate that the fatigue damage can be sensitive to  $L_T$  and  $\Delta_{TP}$ . In particular, it appears that incorrect choice of either  $L_T$  or  $\Delta_{TP}$  can lead to an inaccurate prediction of the maximum damage at the TDZ.

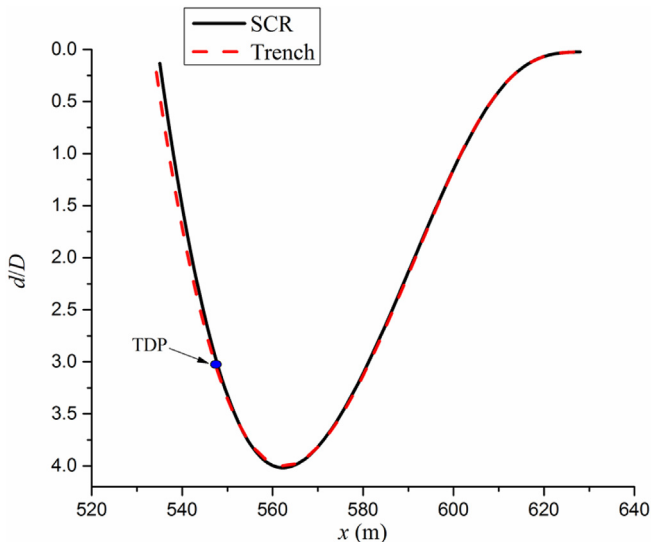


Fig. 7. SCR and trench shapes corresponding to  $d_{\max} = 4D$ .

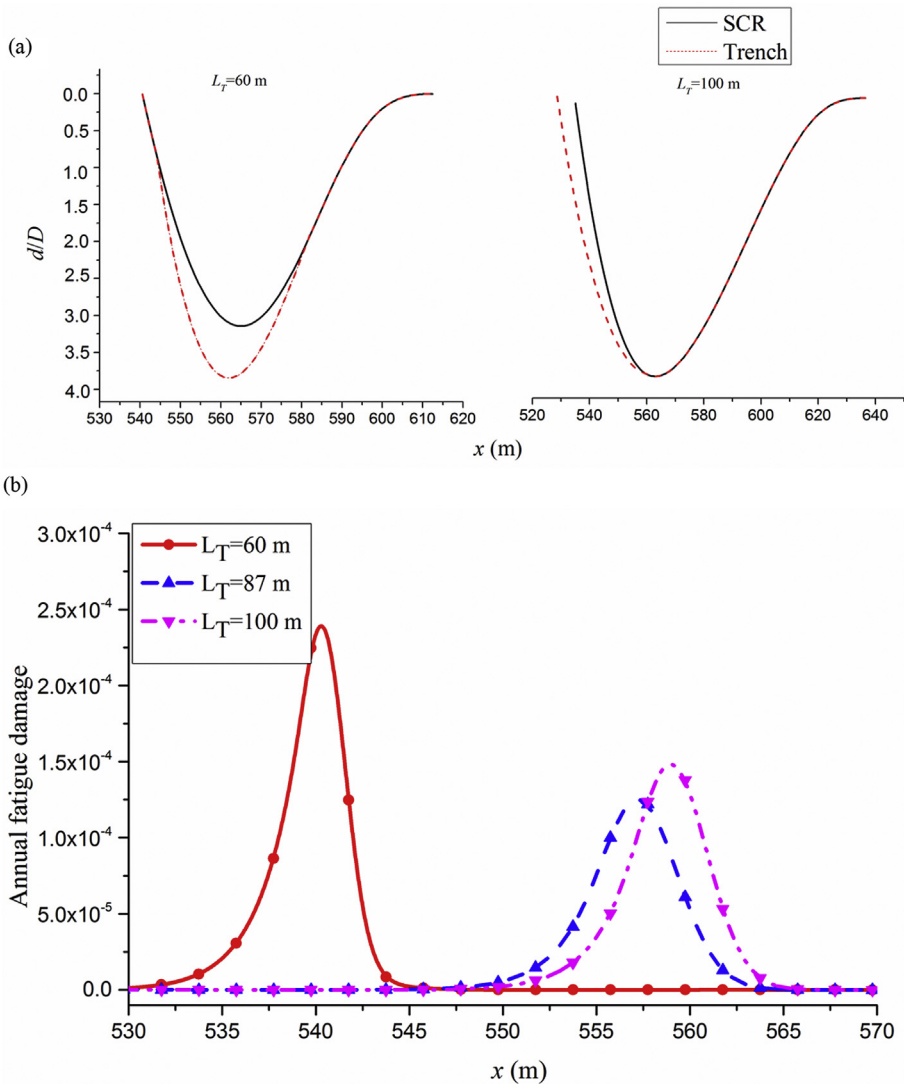


Fig. 8. Effect of varying  $L_T$  on: (a) trench profile; (b) fatigue damage.

#### 4. Proposed trench model

Based on the insights obtained from the preliminary simulations described in Section 3, the proposed parametric trench model will be based on the cubic polynomial. As shown in Section 3, the fatigue damage is sensitive to  $L_T$  and  $\Delta_{TP}$ , thus it is important to assign more verified values for these parameters.

##### 4.1. Iterative static analysis approach

As demonstrated in Section 2.1, the magnitude of the platform motion using the existing models predominantly affects the trench development speed, and has little influence on the trench profile for a

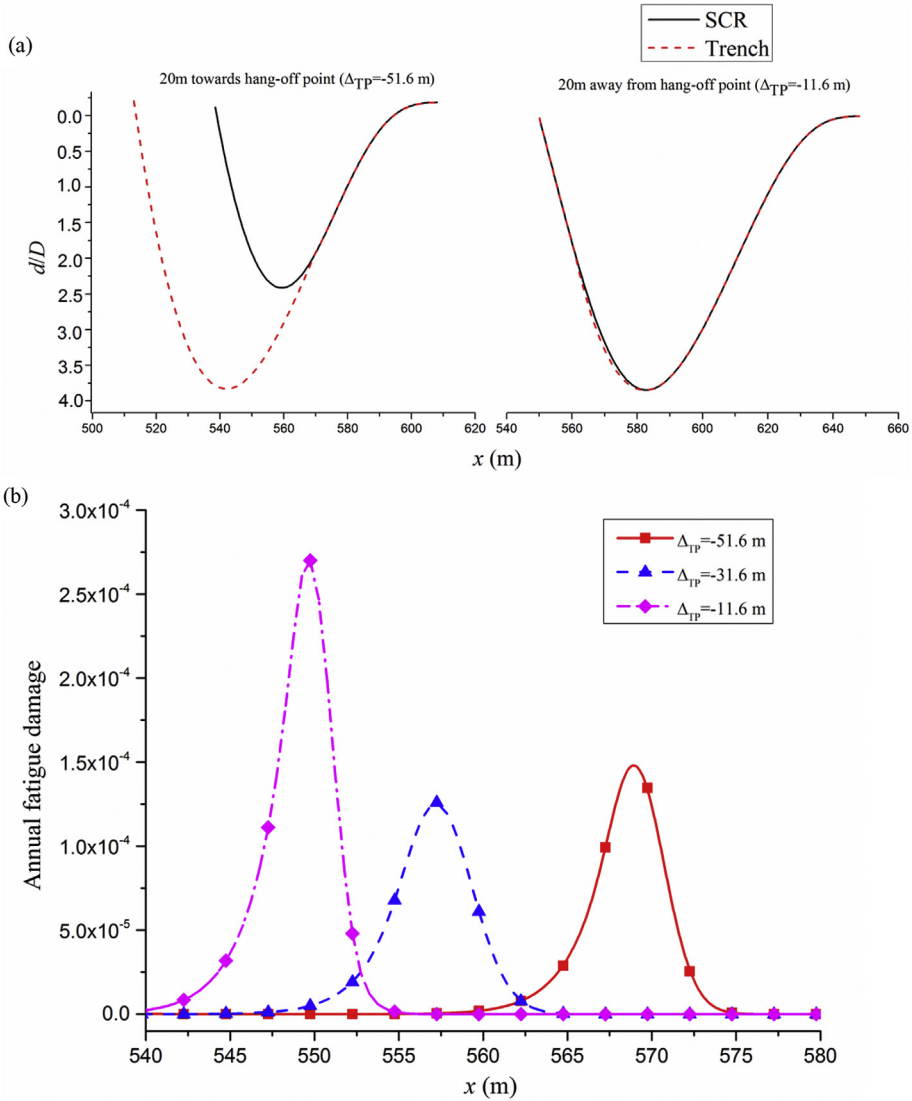


Fig. 9. Effect of varying  $\Delta_{TP}$  on: (a) trench profile; (b) fatigue damage.

given trench depth. Thus, it seems reasonable that the appropriate  $L_T$  and  $\Delta_{TP}$  can be deduced from static considerations alone. In this connection, an original method is proposed for obtaining  $L_T$  and  $\Delta_{TP}$  based on iterative static analysis.

The static analysis procedure is formulated as a constrained optimization problem. Specifically, the shortest possible  $L_T$  is sought, subject to two constraints: (1) The TDP should lie between the TBP and TMP; (2) there must be no gap between the SCR and trench from TDP to TEP. Together, constraints (1) and (2) ensure the trench profile provides a good match with the SCR.

The features of the two constraints are consistent with numerical simulations using the seabed contact model. The left diagram of Fig. 9(a) illustrates the consequences if constraint (1) is not satisfied (however, constraint (2) is fulfilled). As only the rear portion of the trench is in contact in the static

state, that portion of the seabed will have a relatively faster trench development due to more frequent SCR-seabed contact. This may result in a discontinuous trench profile. The right diagram of Fig. 9(a) depicts the scenario where constraints (1) and (2) are both violated. The gap implies that a smaller contact area and larger than usual reactions at the fore end; this will lead to a faster trench development near the TBP, culminating in a situation with no gap.

The impetus for optimizing  $L_T$  is the heuristic argument that for a two-dimensional model, a shorter trench requires less effort to develop, since the reaction forces leading to trench development are distributed over a smaller area resulting in higher seabed reaction stresses. Thus, for various possible trenches with different  $L_T$ , that with the smallest  $L_T$  will be the most natural one. Moreover, the optimization is necessary to ensure a unique solution for a given SCR configuration, otherwise there will be infinite possibilities of  $L_T$  and  $\Delta_{TP}$  that will satisfy the constraints.

To illustrate the problem characteristics, Fig. 10 shows a typical  $L_T - \Delta_{TP}$  domain that is divided into the following regions:

Region A: Both constraints (1) and (2) are satisfied.

Region B: At least one constraint is violated, and the TDP is on the left-hand side of the TMP, typically like the right diagram of Fig. 9(a).

Region C: At least one constraint is violated, and the TDP is on the right-hand side of the TMP, typically like the left diagram of Fig. 9(a).

Fig. 10 corresponds to a specific SCR configuration, however the characteristics should be fairly generic. The  $L_T - \Delta_{TP}$  domain is first partitioned into a regular grid, and static analyses are performed for each cell to determine if the cell belongs to Regions A, B or C according to the aforementioned criteria. Fig. 10 indicates that the larger  $L_T$  is, the wider will be the permissible range of  $\Delta_{TP}$ . There will be an optimal  $L_T$  in which  $\Delta_{TP}$  is restricted to a unique value; this corresponds to the cell labeled as  $A_1$ , which is the optimal point. There may be various strategies to search for the optimal point. The flowchart of the algorithm adopted in this study is shown in Fig. 11. The main features of the iterative procedure are as follows. For any iteration, if the point already lies in Region A, then  $L_T$  is reduced to move towards the optimal solution. If the point lies in either Regions B or C, then  $\Delta_{TP}$  will be increased or decreased respectively, until Region A is reached. However, if the iteration crosses from Region B to C, or vice versa, bypassing Region A, then  $L_T$  will be increased. Finally, if two successive iterations are in Region A and the convergence criterion is fulfilled, then the optimal solution of  $L_T$  and  $\Delta_{TP}$  is considered to be found, and the iterative process is terminated.

To implement the algorithm, an in-house computer code is developed to provide an interface between Orcaflex and C++, so that the iterative static analysis can be performed automatically. At the

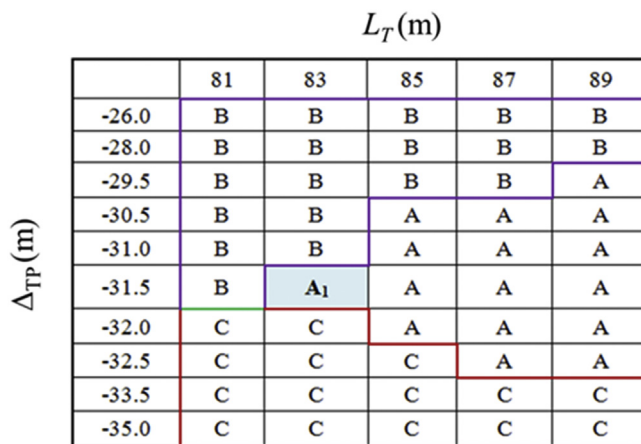


Fig. 10. Domain of  $L_T - \Delta_{TP}$  divided into Regions A, B and C.

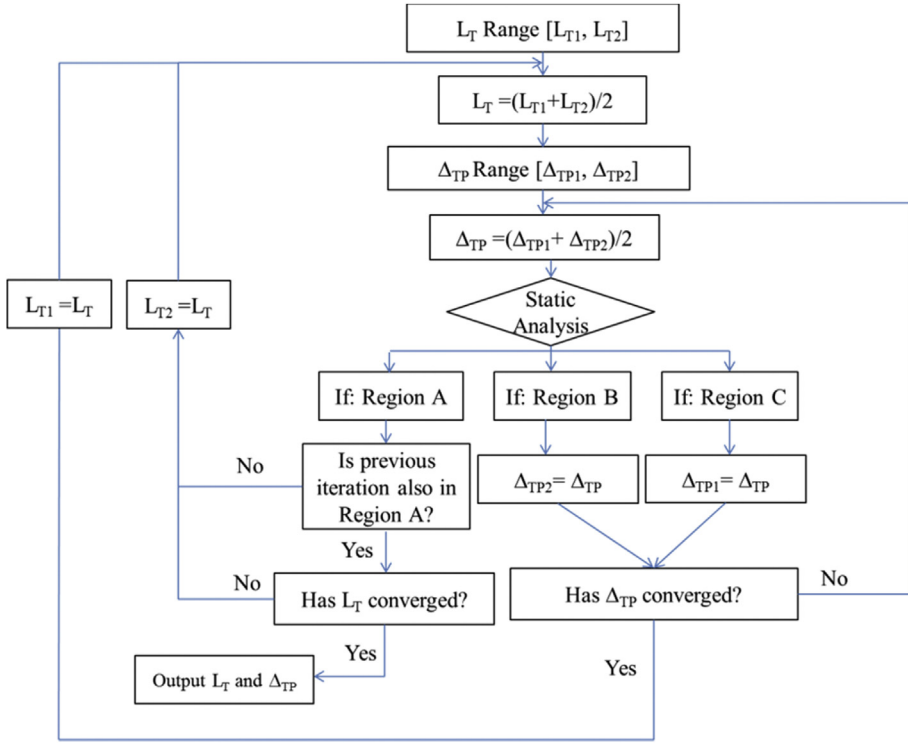


Fig. 11. Flowchart illustrating the iterative algorithm for calculating  $L_T$  and  $\Delta_{TP}$ .

completion of each static analysis, the SCR displacement at the TDZ is extracted, and compared against the seabed profile to check whether the convergence criterion is met.

4.2. Surrogate model

The aforementioned static analysis approach provides a viable alternative for obtaining an initial trench profile, and it is certainly much faster than using the hysteretic seabed model. Nevertheless, the static analysis approach requires iteration and a specialized computer code to implement, making it less appealing for practical applications. For this reason, a simpler approach is proposed, based on establishing a surrogate model, so that  $L_T$  and  $\Delta_{TP}$  can be calculated directly from explicit equations.

It is convenient to normalize  $L_T$  and  $\Delta_{TP}$  by

$$R_L = \frac{L_T}{D}, \quad R_{TP} = \frac{\Delta_{TP}}{D} \tag{5}$$

The input parameters should be dimensionless to allow the surrogate model to be applied to different SCR configurations. The critical non-dimensional parameters influencing  $R_L$  and  $R_{TP}$  are identified as follows:

$$R_d = \frac{d_{max}}{D}, \quad R_M = \frac{M}{\rho \pi D^2 / 4}, \quad R_{HV} = \frac{H}{V} \tag{6}$$

where  $R_d$  is the non-dimensional maximum trench depth,  $R_M$  is the mass ratio (riser mass  $M$  over displaced fluid mass), while  $R_{HV}$  is the ratio of the horizontal distance  $H$  to vertical distance  $V$  between

the hang-off point and TDP for a flat seabed (see Fig. 3). The aim is to approximate  $R_L$  and  $R_{TP}$  as functions of the independent parameters  $R_d$ ,  $R_M$  and  $R_{HV}$ , i.e.

$$R_L = f(R_d, R_M, R_{HV}), \quad R_{TP} = g(R_d, R_M, R_{HV}) \quad (7)$$

To establish the functions  $f(\cdot)$  and  $g(\cdot)$ , trench analyses are performed using the iterative static analysis method, for different combinations of  $R_d$ ,  $R_M$  and  $R_{HV}$ . The parameters of the SCR configuration are given in Table 2. In the analyses, the water depth and  $D$  are kept constant;  $R_d$ ,  $R_M$  and  $R_{HV}$  are varied by changing  $d_{\max}$ ,  $M$  and  $H$  respectively. The values of  $R_d$ ,  $R_M$  and  $R_{HV}$  considered are reported in Table 3. The total number of combinations is 504. Due to space limitations, only selected results are presented and discussed below.

Fig. 12(a)–(c) plots the trends of  $R_L$  against  $R_d$ ,  $R_M$  and  $R_{HV}$ . Referring to Fig. 12(a),  $R_L$  shows an increasing trend with  $R_d$ , an expected outcome since a longer trench should be associated with a deeper one. Fig. 12(b) indicates that  $R_L$  decreases marginally with increasing  $R_M$ . One possibility may be that for the same  $R_L$ , a higher mass will lead to a deeper trench caused by the increased weight; as a corollary, by fixing  $R_d$  instead, higher mass will correspond to lower  $R_L$ . In any case, the effect is very slight. Fig. 12(c) shows an almost linear increase of  $R_L$  with  $R_{HV}$ . The reason is that a larger  $R_{HV}$  corresponds to a smaller trench slope at the TBP. According to Eq. (1), the slope is equal to  $d_{\max}c_3/L_T$ . From Eq. (3), it can be inferred that  $c_3$  is constant, and accordingly a smaller slope will correspond to a longer trench under a constant trench depth.

Fig. 13(a)–(c) show the variation of  $R_{TP}$  with  $R_d$ ,  $R_M$  and  $R_{HV}$ , from which it can be perceived that  $R_{TP}$  is more sensitive to the three parameters, compared to  $R_L$ . It is also observed that  $R_{TP}$  is always negative meaning the TBP is at the left of the TDP associated with flat seabed. Referring to Fig. 13(a), when  $R_{HV}$  and  $R_M$  are constant, the reference position (TDP for flat seabed) is independent of  $R_d$ . Thus, an increase in  $R_d$  is accompanied by a longer trench, causing the TBP to move further away from the reference position; consequently  $R_{TP}$  becomes more negative. The trends for Fig. 13(b)–(c) can likewise be explained by linking the effect to the trench length. For example, as  $R_M$  increases,  $R_L$  decreases as discussed earlier, leading to the TBP moving towards the right (larger  $R_{TP}$ ).

Having the full results, surrogate models can be devised for  $R_L$  and  $R_{TP}$ . The most obvious choice is to fit to multivariate polynomials. For the present situation of three variables, a full second-order polynomial equation entails 10 terms. It is beneficial to have as few terms as possible for simplicity, but accuracy should not be unduly compromised. The optimal number of terms is determined by inspecting the effect of removing each term. Using the technique of multivariate polynomial regression that is based on minimizing the sum of squared residuals [25], the expressions for  $R_L$  and  $R_{TP}$  are obtained as

$$R_L = 72.5 + 30.9R_d + 106.1R_{HV} - 17.2R_M - 3.38R_d^2 + 46.2R_dR_{HV} \quad (8)$$

$$R_{TP} = -99.2 - 12.7R_d + 48.8R_M - 30R_{HV} + 13.5R_d^2 - 8.2R_M^2 - 12.1R_dR_{HV} \quad (9)$$

Figs. 14 and 15 compare the results between iterative static analysis and the surrogate model, with one of the three variable kept constant in each diagram. For both  $R_L$  and  $R_{TP}$  the fitted surfaces appear to match the data points well. The results of the surrogate model are also included in Figs. 12 and 13 as lines. It is observed that there is fairly good agreement between the data points and the fitted result.

**Table 3**

Values of the parameters  $R_d$ ,  $R_M$  and  $R_{HV}$  considered in the iterative static analyses.

Parameter	Values considered
$R_d$	1.5, 2.0, 2.5, 3.0, 3.5, 4.0, 4.5, 5.0
$R_M$	1.4, 1.6, 1.8, 2.0, 2.2, 2.4, 2.6, 2.8, 3.0
$R_{HV}$	0.361, 0.456, 0.560, 0.675, 0.803, 0.954, 1.129

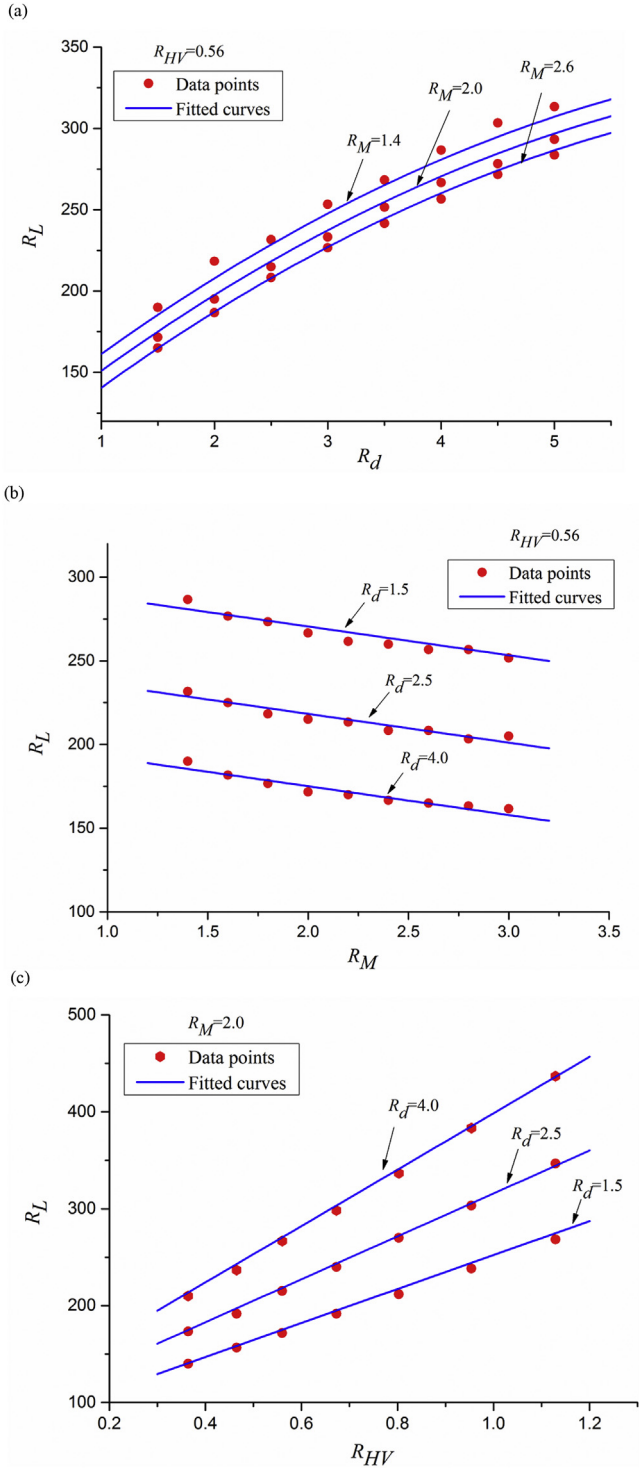


Fig. 12. Variation of  $R_L$  with different parameters: (a)  $R_d$ ; (b)  $R_M$ ; (c)  $R_{HV}$ .

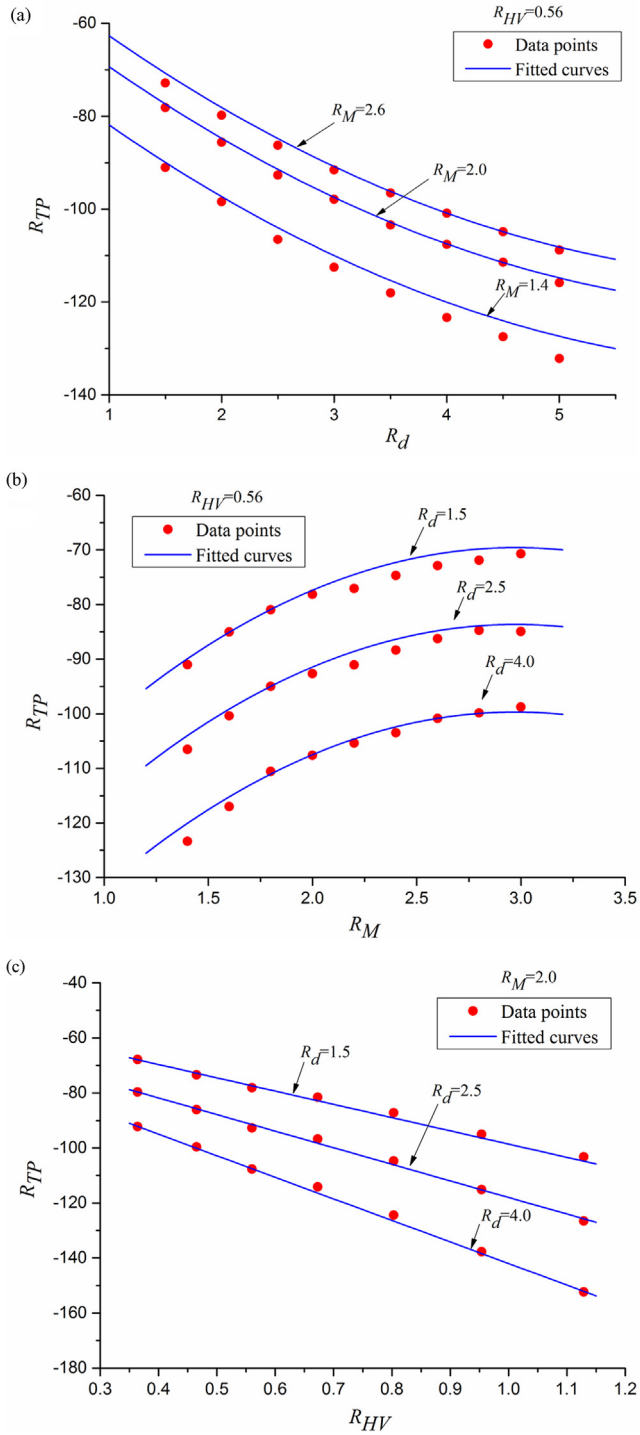
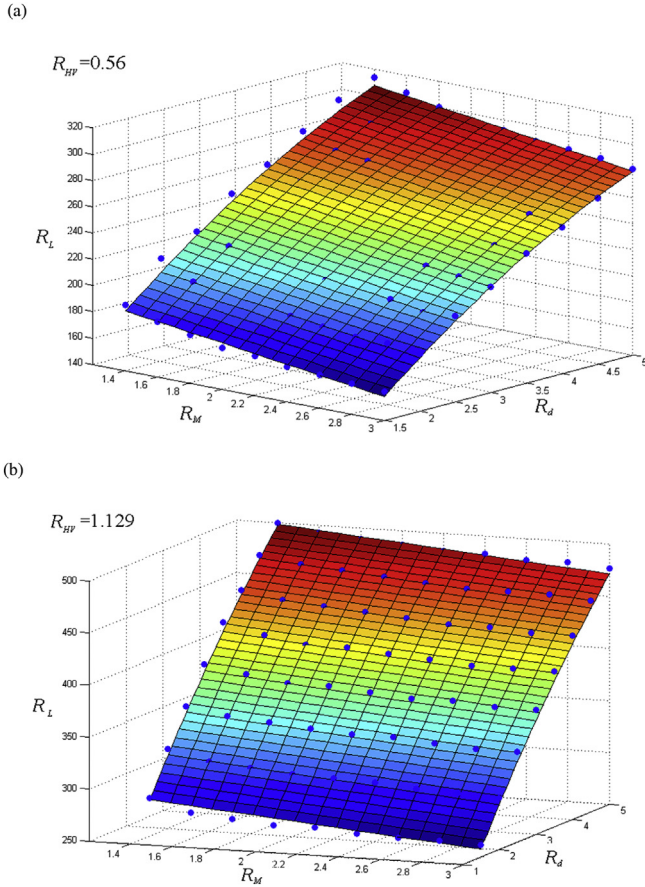


Fig. 13. Variation of  $R_{TP}$  with different parameters: (a)  $R_d$ ; (b)  $R_M$ ; (c)  $R_{HV}$ .



**Fig. 14.** Surface plots of  $R_L$  as a function of  $R_M$  and  $R_d$ : (a)  $R_{HV} = 0.56$ ; (b)  $R_{HV} = 1.129$ .

The goodness-of-fit is often characterized by the coefficient of determination  $R^2$ , which ranges from 0 to 1, with a higher  $R^2$  indicating a better fit. For  $R_L$ , the  $R^2$  values are 0.998 and 0.995 for the full second-order polynomial and Eq. (8) respectively, whereas for  $R_{TP}$   $R^2 = 0.997$  and 0.995 for the full second-order polynomial and Eq. (9) respectively. These results imply that Eqs. (8) and (9) are virtually as accurate as the full second-order polynomials despite omitting some terms. In both Eqs. (8) and (9), there are mixed terms involving  $R_d$  and  $R_{HV}$ , signifying that the interactions between these two terms have significant influence on the trench length and position.

The parameters  $R_d$ ,  $R_M$  and  $R_{HV}$  do not fully define an arbitrary SCR configuration; an additional parameter is needed to represent the riser bending stiffness,  $EI$ . However, with four parameters, the computational effort to set up the database is prohibitive, and the resulting equations will be much more complicated. A simple parametric study has been performed to assess the importance of varying  $EI$ , with  $R_d = 4$ ,  $R_{HV} = 0.56$ , and  $R_M = 2.6$ . It is found that when  $EI$  is increased twofold from the default value of  $3.0 \times 10^7 \text{ Nm}^2$ ,  $R_L$  increases by 10%, while  $R_{TP}$  diminishes by 10%. These discrepancies are much smaller than those originating from  $R_d$ ,  $R_M$  and  $R_{HV}$ . For this reason, the effect due to the variation of  $EI$  is neglected for simplicity.

#### 4.3. Validation and discussion

It is important to verify the proposed trench model, which is based on static analysis, by comparison with the numerical trench produced by dynamic analysis in conjunction with the nonlinear seabed

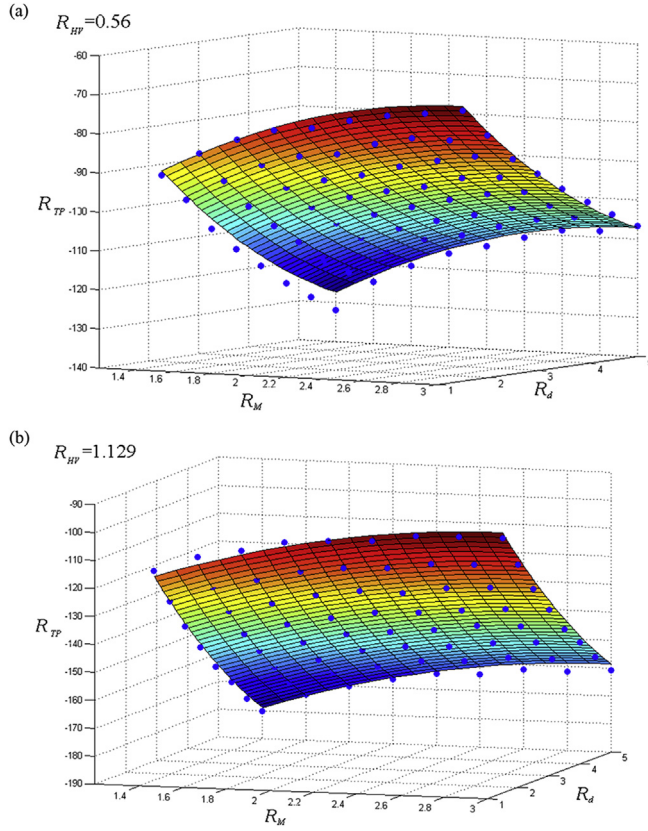


Fig. 15. Surface plots of  $R_{TP}$  as a function of  $R_M$  and  $R_d$ : (a)  $R_{HV} = 0.56$ ; (b)  $R_{HV} = 1.129$ .

contact model. The numerical trench results are obtained from two sources, namely (1) simulations performed by Shiri and Randolph [15], and (2) new dynamic simulations performed in this study.

Shiri and Randolph [15] implemented the nonlinear hysteretic seabed in the commercial software ABAQUS and obtained a series of trenches with  $R_{HV} = 0.625$  and  $R_M = 1.2$  approximately. For the present dynamic simulations, the seabed contact parameter  $\lambda_{rep}$  is assigned to be 1.5 to obtain a deeper trench for the same simulation duration, since a large  $\lambda_{rep}$  represents a faster trench development [15]. The simulation duration required to reach the desired trench depth is approximately 150 h.

Table 4 compares  $R_L$  and  $R_{TP}$  obtained by the numerical trench and the proposed surrogate model (i.e. Eqs. (8) and (9)). The results of  $R_L$  and  $R_{TP}$  from the present numerical simulations are close to the

**Table 4**  
Comparison of  $R_L$  and  $R_{TP}$  obtained by numerical trench and proposed surrogate model.

	$R_d$	$R_L$		$R_{TP}$	
		Numerical results	Surrogate model	Numerical results	Surrogate model
Shiri and Randolph [15]	2.70	280.8	254.9	-110.2	-116.1
$R_{HV} = 0.625, R_M = 1.2$	4.00	331.5	303.2	-124.3	-130.6
Present study	2.60	228.8	218.8	-86.2	-89.8
$R_{HV} = 0.56, R_M = 2.2$	4.30	280.4	275.7	-104.5	-107.1
Present study	1.75	221.5	228.5	-87.5	-90.7
$R_{HV} = 0.803, R_M = 2.2$	3.40	311.3	312.0	-113.3	-116.2

proposed approach; the small differences may be induced by the discrepancy in shape between the cubic equation and the numerical trench; see Fig. 5. There is slightly larger disparity between Shiri and Randolph's results and the proposed approach, especially in  $R_L$ . This may be attributed to the difference in soil stiffness used in the two studies. In Shiri and Randolph, the mudline shear strength  $S_{U0}$  is set to 0.6 kPa, which differs from that used in the present study. Nevertheless, the relatively good agreement indicates that the seabed stiffness has minimal impact on the trench.

Fig. 16 compares the trench profiles with  $d_{\max} = 4.3D$ , obtained by three approaches, namely (i) numerical trench simulated in this work, (ii) iterative static analysis, and (iii) surrogate model. Overall, the three trench profiles are in good agreement, although the parametric models (i.e. (ii) and (iii)) appear to be somewhat broader compared to the numerical trench.

Ultimately, the critical test of the viability of the proposed approach still lies in a fatigue analysis, since it is the fatigue performance that is of concern. In this connection, fatigue analyses are performed using the three trench profiles, in addition to a flat elastic seabed case, and the fatigue damage results at the TDZ are plotted in Fig. 17. It can be perceived that the fatigue response with flat seabed is vastly dissimilar from the cases with trench. The TDP for flat seabed is different, and this affects the location of the maximum damage. In addition, the maximum damage is also conservative in comparison with the cases with trench, indicating that the trench is beneficial for the fatigue life of an SCR. This observation is consistent with much of the published literature (e.g. Refs. [2,20]). Nevertheless, there are also some studies (e.g. Ref. [8]) reporting that the trench can be detrimental to the fatigue life. Focusing now on the trench cases, the iterative static analysis and surrogate model match the numerical trench very well, both in terms of the peak damage as well as its location along the SCR. The results suggest that the parametric models may yield a slightly conservative estimate of the fatigue damage. However, overall the proposed trench model is acceptable, and can be used for prediction of the fatigue damage at the TDZ.

In the proposed model,  $d_{\max}$  is assumed to be known, but in practical design, it needs to be specified by the engineer. Unfortunately, there is no simple solution, but several options are possible; for example it can be inferred from field measurements of existing comparable SCR configurations and soil properties. In the absence of field data, a range of typical  $d_{\max}$  (e.g.  $4D$  to  $5D$ ) can be considered in fatigue analysis, and the most critical value is used for design. Finally,  $d_{\max}$  can be recognized as a source of uncertainty, and modeled as a random variable in a fatigue reliability analysis as proposed in a recent study [26].

It is useful to place the contribution of this study in the broader context. It is highlighted that the fatigue performance of an SCR at the TDZ is an extremely intricate topic with a wide range of inherent

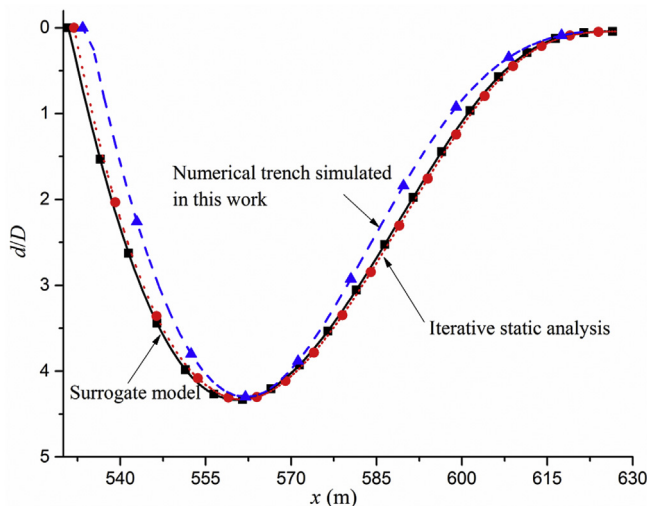


Fig. 16. Comparison of trench profiles by different models.

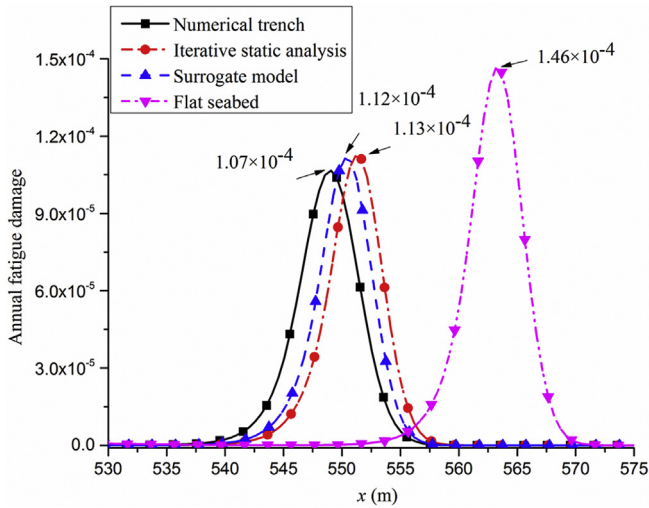


Fig. 17. Comparison of fatigue damage near TDP using different trench models.

uncertainties. The fatigue behavior depends not only on the trench and soil properties (which are by themselves complex and uncertain), but also on many other physical mechanisms that are still not well understood, such as the surrounding fluid velocity field, scour around the riser, vortex-induced vibration, and low-frequency vessel motions. Despite many high quality experimental and numerical studies, there is still no robust convergence regarding the impact of seabed trench on fatigue life. Hence, this work represents an attempt to find a simple solution to a complex problem, and it still requires further validation. In addition, the low frequency drift motions, which have been neglected in the proposed model, are known to have profound influence on the trench, and on the fatigue life at the TDZ [19]. For one thing, the low-frequency motions spread the TDP over a wider region, resulting in a broader trench. Incorporating the low-frequency motions into the proposed model increases the complexity markedly, because additional parameters have to be introduced; nevertheless, this is a potential area for future work.

## 5. Conclusions

Research studies [18] have indicated that the seabed trench profile significantly affects the fatigue performance of an SCR at the touchdown zone, and this is further verified by preliminary simulations performed in this work. The nonlinear hysteretic seabed contact model [11] is presently the most well-regarded available method for simulating trench development arising from repeated cycles of riser-soil contact. However, in practical design, it is time consuming to employ this numerical model to obtain an initial trench profile for time domain fatigue analysis.

This paper presents a new simple formulation for delineating an initial trench profile. This formulation is based on a cubic polynomial equation, which is herein demonstrated to be a suitable parametric model, by comparison with the numerically simulated trench. The cubic polynomial trench entails only two parameters, namely the trench length  $L_T$  and trench position  $\Delta_{TP}$ . It is shown that the fatigue performance is highly sensitive to both  $L_T$  and  $\Delta_{TP}$ . An iterative static analysis method is proposed for obtaining reasonable values of  $L_T$  and  $\Delta_{TP}$  by solving a constrained optimization problem.

Nevertheless, the iterative static analysis is complicated and not ideal for practical applications. Hence, a surrogate model is devised, by approximating  $L_T$  and  $\Delta_{TP}$  as multi-variate polynomial functions of three dimensionless parameters  $R_d$ ,  $R_M$ ,  $R_{HV}$ . A database of results is set up by performing the iterative static analysis for various combinations of  $R_d$ ,  $R_M$ ,  $R_{HV}$ , and the coefficients of the polynomial functions are determined by regression analysis. The surrogate model fits the data well, with  $R^2$  values

of 0.995 for both  $L_T$  and  $\Delta T_P$ . A case study shows that the trench profiles obtained by the numerical model, iterative static analysis, and surrogate model are in good agreement. Moreover, dynamic analyses are carried out, and the maximum fatigue damages associated with different trenches are found to be very close.

Finally, it is highlighted that the fatigue performance of an SCR at the touchdown zone is influenced by a multitude of inherently uncertain physical mechanisms that are still not well understood. This work represents an attempt to find a reasonable simple model to a complex problem, and it still requires further validation.

## Acknowledgments

The authors gratefully acknowledge the financial support from NUS Start-up Grant, No. R-302-000-099-133.

## References

- [1] Bridge C, Laver K. Steel catenary riser touchdown point vertical interaction models. In: Proceedings of the offshore technology conference, Houston, Texas; 2004.
- [2] Nakhaee A, Zhang J. Trenching effects on dynamic behavior of a steel catenary riser. *Ocean Eng* 2010;37(2–3):277–88.
- [3] Bridge C, Howells H, Toy N, Parke G, Woods R. Full-scale model tests of a steel catenary riser. *Fluid structure interaction II*. WIT Press; 2003.
- [4] Elliott BJ, Zakeri A, Barrett J, Hawlader B, Li G, Clukey EC. Centrifuge modeling of steel catenary risers at touchdown zone part II: assessment of centrifuge test results using kaolin clay. *Ocean Eng* 2013;60:208–18.
- [5] Wang L, Zhang J, Yuan F, Li K. Interaction between catenary riser and soft seabed: large-scale indoor tests. *Appl Ocean Res* 2014;45:10–21.
- [6] Sen TK, Hesar M. Riser soil interaction in soft clay near the touchdown zone. In: Proceedings of the offshore technology conference, Houston, Texas; 2008.
- [7] Clukey E, Jacob P, Sharma P. Investigation of riser seafloor interaction using explicit finite element methods. In: Proceedings of the offshore technology conference, Houston, Texas; 2008.
- [8] Aubeny CP, Biscontin G. Interaction model for steel compliant riser on soft seabed. In: Proceedings of the offshore technology conference, Houston, Texas; 2008.
- [9] Aubeny CP, Biscontin G. Seafloor-riser interaction model. *Int J Geomech* 2009;9:133–41.
- [10] Bai X, Huang W, Vaz MA, Yang C, Duan M. Riser-soil interaction model effects on the dynamic behavior of a steel catenary riser. *Mar Struct* 2015;41:53–76.
- [11] Randolph M, Quiggin P. Non-linear hysteretic seabed model for catenary pipeline contact. In: Proceedings of the 28th international conference on ocean, offshore and arctic engineering, Honolulu, Hawaii, vol. 3; 2009. p. 145–54.
- [12] Aubeny CP, Gaudin C, Randolph M. Cyclic tests of model pipe in Kaolin. In: Proceedings of the Offshore Technology Conference, Houston, Texas; 2008.
- [13] Elostalo H, Huang S, Incecik A. Dynamic response of steel catenary riser using a seabed interaction under random loads. *Ocean Eng* 2013;69:34–43.
- [14] Elostalo H, Huang S, Incecik A. Trenching effects on structural safety assessment of integrated riser/semisubmersible in cohesive soil. *Eng Struct* 2014;77:57–64.
- [15] Shiri H, Randolph M. The influence of seabed response on fatigue performance of steel catenary risers in touchdown zone. In: Proceedings of the 29th international conference on ocean, offshore and arctic engineering, Shanghai, vol. 5; 2010. p. 63–72.
- [16] Shiri H. Response of steel catenary risers on hysteretic non-linear seabed. *Appl Ocean Res* 2014;44:20–8.
- [17] Willis NRT, West PTJ. Interaction between deepwater catenary risers and a soft seabed: large scale sea trials. In: Proceedings of the offshore technology conference, Houston, Texas; 2001.
- [18] Shiri H. Influence of seabed trench formation on fatigue performance of steel catenary risers in touchdown zone. *Mar Struct* 2014;36:1–20.
- [19] Li FZ, Low YM. Influence of low-frequency vessel motions on the fatigue response of steel catenary risers at the touchdown point. *Ships Offsh Struct* 2014;9(2):134–48.
- [20] Bridge C, Howells HA. Observations and modeling of steel catenary riser trenches. In: Proceedings of the Seventeenth International Offshore and Polar Engineering Conference, Lisbon, Portugal; 2007.
- [21] Det Norske Veritas. DNV-RP-C205 Environmental conditions and environmental loads. 2010.
- [22] Det Norske Veritas. DNV-RP-C205 Fatigue design of steel offshore structures. 2011.
- [23] Downing SD, Socie DF. Simple rainflow counting algorithms. *Int J Fatigue* 1982;4(1):31–40.
- [24] Miner MA. Cumulative damage in fatigue. *J Appl Mech* 1945;12(3):159–64.
- [25] Rencher AC, Christensen WF. *Methods of multivariate analysis*. 3rd ed. Wiley; 2012.
- [26] Li FZ, Low YM. Fatigue reliability analysis of a steel catenary riser at the touchdown point incorporating soil model uncertainties. *Appl Ocean Res* 2012;38:100–10.